DOI: 10.1002/ejic.201101301

Heterometallic Complexes of Ruthenium and Lanthanides (Ce, Pr, Nd, Eu) with NO_2 Bridges – Synthesis, Structures, Properties

A. O. Borodin,[a] G. A. Kostin,*[a,b] P. E. Plusnin,[a,b] E. Yu. Filatov,[a,b] A. S. Bogomyakov,[c] and N. V. Kuratieva[a,b]

Keywords: Ruthenium / Rare earths / Heterometallic complexes / Thermal decomposition / Magnetic properties

Five new heterometallic complexes with a {Ln[RuNO(μ-NO_2)$_4$-(μ$_3$-OH)]$_2$Ln} (Ln = Ce, Pr, Nd, Eu) core were prepared by reaction of Na_2[RuNO(NO_2)$_4$OH] and lanthanide nitrates in the presence of pyridine. The crystal structures of the obtained compounds were determined by single-crystal X-ray analysis. In all complexes, Ru and Ln atoms are connected by N,O-bridging nitrite groups and OH groups. The coordination environment of Ln^{3+} is completed by oxygen atoms of nitrate ions and water molecules and by nitrogen atoms of pyridine molecules. Magnetic interactions between lanthanide atoms become apparent at temperatures lower than 40–50 K, and at temperatures higher than 100 K, the dependencies of the magnetic susceptibilities of the complexes are well explained by the presence of two noninteracting paramagnetic centers. Thermal decomposition of the investigated complexes in an inert atmosphere results in a mixture of metallic ruthenium and the corresponding lanthanide oxide. Formation of mixed oxide phases $RuPrO_x$ was also detected after decomposition of the praseodymium complex.

Introduction

Interest in ruthenium nitrosyl complexes including heteronuclear species is determined by the unique properties of these compounds. The ability to undergo reversible light-induced transformation to long-lived metastable isomers[1] can be used for designing new photo-switching devices for information storage.[2] Combined with paramagnetic centers, ruthenium nitrosyl complexes are interesting as building blocks for the synthesis of bifunctional materials with both photochromic and magnetic properties. Several attempts were made to combine RuNO complexes with the paramagnetic center of another metal:[3] reversible photomagnetism was found for double-salt complex [RuNO(NH_3)$_5$][Cr(CN)$_6$] and for the double salt of [RuNO(NH_3)$_4$-OH]$^{2+}$ and Gd^{3+} with the thiacalixarene anion. From this point of view, combination of the RuNO fragment with luminescent and paramagnetic lanthanides in one complex would be interesting because of the mutual influence of the two metals.

Another promising direction in the chemistry of heterometallic Ru–Ln complexes is related to the development of functional materials based on metallic ruthenium or mixed Ru–Ln oxides. Catalytic systems such as Ru–CeO_2 are intensively investigated in the processes of hydrogen preparation and purification.[4] Doping of the oxide supporting phase in Ru/Fe_2O_3 catalyst with different lanthanides (La, Sm) results in an increase in the CO conversion.[5] Mixed oxides of ruthenium and lanthanides, also doped with other elements, are mainly interesting because of their magnetic properties. Oxides with a $Ln_2Ru_2O_7$ pyrochlore-type structure possess spin-glass properties;[6] perovskite-like ternary oxides $MLn_xRu_{1-x}O_3$ (M = Ca–Ba) can have different magnetic behavior depending on the lanthanide and the structure;[7] $RuSr_2LnCu_2O_8$ has both ferromagnetic and superconductivity properties.[8] At present, the systems mentioned above are prepared from components containing each metal separately. This allows the easy variation of the desired composition but at the same time requires a high-temperature synthesis (up to 900 °C in the case of mixed oxides). A promising method is the use of heterometallic precursors – complexes already containing two (or more) different metals. Thermal decomposition of these precursors usually occurs at lower temperatures, and the composition defined at the molecular level determines the stoichiometry of the final products. Work in this area is mainly devoted to double complex salts of nitrosyl ruthenium cations.[9]

Thus, the scientific interest in the development of new ruthenium compounds with other transition metals, including lanthanides, and the urgency of this problem is not to be doubted. However, it should be noted that investigations in this area are mainly focused on the synthesis of double complex salts, in which the counterions containing different metals are connected only by electrostatic interaction. Pre-

[a] Institute of Inorganic Chemistry,
av. Lavrentyeva, 3, Novosibirsk, Russian Federation
E-mail: kostin@niic.nsc.ru
[b] Novosibirsk State University,
str. Pirogova, 2, Novosibirsk, Russia
[c] International Tomography Center,
str. Institutskaya, 3A, Novosibirsk, Russia

Supporting information for this article is available on the WWW under http://dx.doi.org/10.1002/ejic.201101301.

viously, we proposed a simple technique for the synthesis of heterometallic complexes of the first-row transition metals with the anion $[RuNO(NO_2)_4OH]^{2-}$ (An^{2-}) as one of the ligands and show that the thermal decomposition of these compounds can be used to obtain solid solutions of Ru–M, including the metastable ones.[10] In this paper, the technique has been used for the synthesis of heterometallic ruthenium complexes with lanthanides.

Results and Discussion

In contrast to the previously obtained binuclear complexes with M^{2+} cations (Cu, Zn, Co, Ni), interaction of lanthanide (Ce, Pr, Nd, Eu) nitrates with $Na_2[RuNO(NO_2)_4OH]\cdot 2H_2O$ in the presence of pyridine leads to tetranuclear complexes, in which the pair of lanthanide atoms are bonded by a pair of $[RuNO(NO_2)_4OH]^{2-}$ anions with participation of all four nitro groups and the OH group of each anion (Figure 1). The two lanthanide atoms, a ruthenium atom, and the bridging oxygen atom of the OH group lie nearly in a plane. The deviation of the central oxygen atom from the $RuLn_2$ plane is no more than 0.1 Å, and the central angles M–O–M are in the range 111°–122°. The angles between the Ru1–Ln3–Ln4 and Ru2–Ln3–Ln4 planes are within 36.6° (Ln = Pr; **2**) to 37.9° (Ln = Eu; **5**).

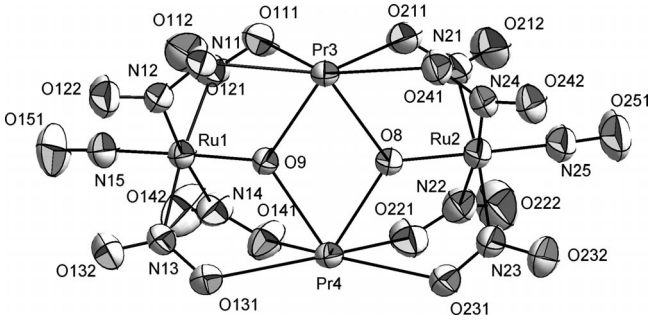

Figure 1. Coordination of lanthanide atoms by the $[RuNO(NO_2)_4OH]$ anion in the obtained complexes.

The average $Ru–N_{NO2}$ distances in complexes **1**–**3** and **5** are slightly shorter than those in the initial anion (Table 1). Only in complex **4** are these distances noticeably larger (2.181 Å). On the contrary, the $Ru–O_{OH}$ distances in all complexes are smaller than those in the original anion, and in case of **4** the distance $Ru–O_{OH}$ is also the largest among those in the remaining complexes. The most interesting is the change in the geometry of the $RuNO^+$ fragment. In previously described Ru/M complexes of nonferrous metals,[10] Ru–N distances are slightly shorter and N–O bond lengths are greater as compared with those of the anion, the Ru–O distances and Ru–N–O angles remaining practically unchanged. In the studied lanthanide complexes there is a simultaneous increase in both bond lengths (0.01–0.04 Å for Ru–NO, and up to 0.1 Å for N–O in complexes **4** and **5**) and the Ru–N–O bond angle (177.0–178.7°). (Selected distances are shown in Tables 1 and 2.)

Table 1. Bond lengths in the ruthenium fragment and M–M distances in complexes **1**–**5**. (Average distances are bold).

Bond		1	2	3	4	5	An^{2-}
$Ru–N_{NO}$	1	1.771(2)	1.772(1)	1.774(1)	1.797(1)	1.779(3)	1.764(2)
	2	1.771(1)	1.769(1)	1.781(1)	1.808(1)	1.773(3)	
$Ru–N_{NO2}$	1	**2.086**	**2.088**	**2.082**	**2.181**	**2.080**	**2.091**
	2	**2.082**	**2.090**	**2.090**	**2.172**	**2.083**	
$Ru–O_{OH}$	1	1.887(2)	1.888(2)	1.880(3)	1.918(1)	1.883(4)	1.962(2)
	2	1.884(2)	1.888(1)	1.886(3)	1.924(1)	1.870(4)	
$N_{NO}–O_{NO}$	1	1.148(2)	1.134(1)	1.140(3)	1.160(3)	1.154(5)	1.135(3)
	2	1.144(2)	1.151(1)	1.150(3)	1.181(3)	1.151(5)	
Ru–M	1	3.743(7) 3.755(8)	3.725(1) 3.739(1)	3.728(2) 3.720(2)	3.852(4) 3.783(5)	3.673(2) 3.673(1)	–
	2	3.730(9) 3.717(6)	3.717(5) 3.699(9)	3.690(3) 3.705(3)	3.798(3) 3.841(2)	3.673(2) 3.662(3)	
		3.736	**3.720**	**3.711**	**3.819**	**3.670**	
Ru–Ru		6.152(5)	6.140(1)	6.117(3)	6.236(8)	6.071(9)	
M–M		3.892(3)	3.861(2)	3.857(2)	4.028(2)	3.767(4)	

Table 2. Bond lengths in the lanthanide environment for complexes **1**–**5**.

Bond		1	2	3	4	5
$Ln–O_{NO2}$	1	2.543(2) 2.668(2) 2.608(1) 2.658(1)	2.589(2) 2.535(1) 2.646(2) 2.667(1)	2.507(2) 2.561(1) 2.562(1) 2.626(2)	2.598(2) 2.618(3) 2.649(2) 2.682(3)	2.541(2) 2.508(2) 2.472(1) 2.564(3)
	2	2.590(2) 2.556(2) 2.607(3) 2.659(2)	2.538(4) 2.567(1) 2.591(4) 2.652(1)	2.511(4) 2.591(2) 2.639(2) 2.641(5)	2.609(1) 2.648(1) 2.671(1) 2.673(1)	2.513(1) 2.540(1) 2.549(3) 2.593(3)
$Ln–O_{NO2}$ (av)		**2.598**	**2.611**	**2.580**	**2.644**	**2.535**
$Ln–O_{OH}$	1	2.337(1) 2.377(0)	2.318(2) 2.350(1)	2.315(2) 2.319(2)	2.384(4) 2.438(2)	2.270(8) 2.285(7)
	2	2.329(1) 2.344(0)	2.318(2) 2.325(1)	2.314(1) 2.347(1)	2.395(4) 2.441(2)	2.284(8) 2.276(7)
$Ln–O_{OH}$ (av)		**2.328**	**2.347**	**2.324**	**2.415**	**2.279**
$Ln–N_{Py}$		2.684(3)	2.678(7)	2.643(5)	2.795(8)	2.600(9)
$Ln–O_{NO3}$	1	2.587(2) 2.606(3) 2.764(1) 2.645(2)	2.594(1) 2.590(2) 2.647(5) 2.775(8)	2.561(3) 2.565(3) 2.614(8) 2.716(9)	2.731(3) 2.684(2)	2.550(2) 2.483(2)
	2	2.587(4) 2.611(5)	2.567(3) 2.603(3)	2.547(5) 2.586(3)	2.631(2) 2.639(3)	2.478(1) 2.528(1)
$Ln–O_{NO3}$ (av)		**2.629**	**2.633**	**2.598**	**2.671**	**2.510**
$Ln–O_{H2O}$		–	–	–	2.558(3)	2.421(9)

Depending on the nature of the lanthanide, the complexes form two types of Ru/Ln units, differing in the coordination environment of one of the lanthanide atoms. In structure **I** (Figure 2), the coordination environment of Ce2 is formed by four oxygen atoms of bridging nitro groups, two oxygen atoms of OH groups, and four oxygen atoms of two nitrate ions. The coordination number is equal to 10. In structure **II**, the coordination sphere of Eu2 includes six oxygen atoms of bridging NO_2 and OH groups, two oxygen atoms of one nitrate ion, and one oxygen atom of the water molecule. The coordination number of Eu2 is equal to 9. The coordination environments of Ce1 and Eu1 in structures **I** and **II**, respectively, are the same – six oxygen atoms

of bridging NO_2 and OH groups, two oxygen atoms of one nitrate ion, and one nitrogen atom of the pyridine molecule. The coordination number is equal to 9.

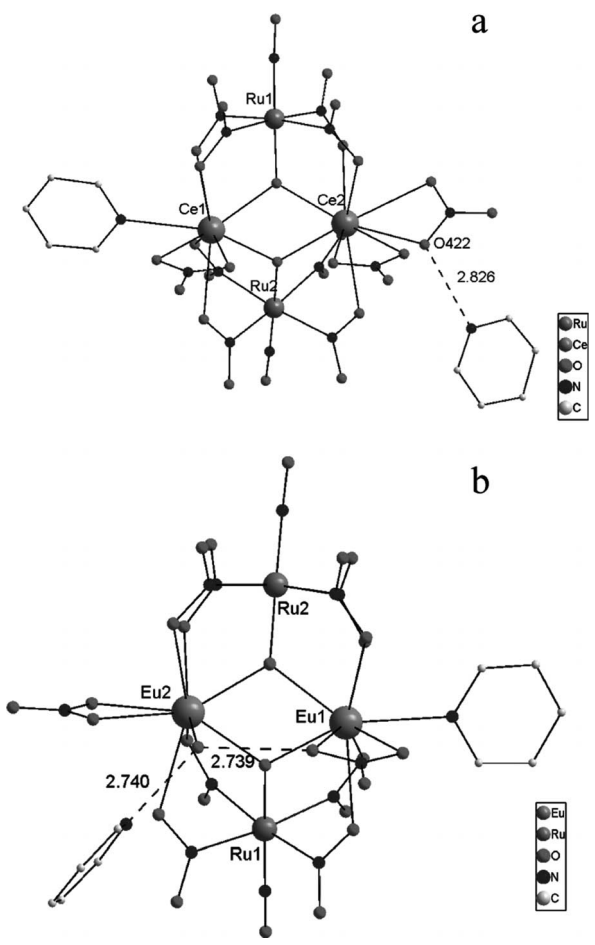

Figure 2. Structure of type **I** (a) and type **II** (b) complexes. Shown are molecules of pyridine coordinated or hydrogen-bonded to the complex core.

The average distance between lanthanide atoms and ligands decreases in the sequence Ce > Pr > Nd for structure **I** and Nd > Eu for structure **II**, corresponding to the decrease in the ionic radii of Ln^{3+}. The change from structure **I** to structure **II** in the neodymium complexes is accompanied by an increase in the average distance between Nd and the ligands.

Regardless of the solvent used in the synthesis (CH_2Cl_2 or acetone), only a complex of structure **I** was obtained for cerium and praseodymium. For neodymium, it was possible to isolate complexes of both types, and in this case, an interesting specificity to the solvent was detected. The complex of structure **I** was formed in acetone as the only reaction product, while in dichloromethane, separate crystals of structure **II** could also be isolated from the reaction mixture by slow diffusion. It should be noted that the solubility of all complexes in dichloromethane is significantly worse than that in acetone, resulting in lower yields due to the coprecipitation of the complexes with $NaNO_3$.

Participation of all four nitro groups of the ruthenium fragment in coordination to the lanthanide atoms is confirmed by the IR spectra of the compounds. In contrast to binuclear complexes $[RuNO(NO_2)_4OHML_n]$ (M = Co, Ni, Zn, Cu), IR spectra of the lanthanide complexes contain only one absorption band for each of NO_2 stretching vibration (ν_{as} and ν_s). The large splitting ($\nu_{as} - \nu_s$ = 154–158 cm^{-1}) corresponds to the unsymmetrical bridging coordination mode. The ν(NO) band for the nitrosyl fragment in the spectra of **1**–**5** is shifted to lower energy by 20–40 cm^{-1} as compared with that in the initial $Na_2[RuNO(NO_2)_4OH]$. In binuclear complexes studied earlier,[10] the shift does not exceed 10 cm^{-1}, which correlates with a bigger distortion of the Ru–NO fragment in the lanthanide complexes. Retention of the OH group of the ruthenium fragment after coordination to the lanthanide atom is confirmed by the broad band of OH vibrations with a maximum in the region 3490–3510 cm^{-1} for complexes of type **I**. In complexes of type **II**, this band overlaps with the stretching vibration band of the coordinated water molecule.

According to data on magnetic moments shown in Table 3, lanthanide atoms in heterometallic complexes maintain an oxidation degree equal to +3. According to this and taking into account the structural studies, elemental analysis, and IR spectra, the total charge of complex fragment $[(NO_3)_2Ln(An)_2Ln(NO_3)Py]$ in structure **I** is equal –1, while the complex fragment $[(H_2O)(NO_3)Ln(An)_2Ln(NO_3)Py]$ in structure **II** is neutral. Since compounds of structure **I** do not contain cations of other metals, we suppose that they should contain H^+ as counterion. The most probable position of this proton is between oxygen atom O422 of the coordinated nitrate ion and the solvated pyridine molecule (Figure 2). For all three compounds of structure **I**, the distance O422–N is short enough for hydrogen bonding (2.82–2.99 Å). In compounds of structure **II**, short contacts of this kind are absent. Intra- and intermolecular hydrogen bonds formed by the coordinated water molecule are shown in the figure.

Table 3. Magnetic moments (Bohr magnetons) and parameters of Curie–Weiss equations for complexes.

Complex	μ_{eff} at 300 K (B.M.)	μ_{eff} at 5 K (B.M.)	μ_{eff}^{calc} (B.M.)	$\chi = C/(T+\theta)$ at 120–300 K	
				C (cm^3K/mol)	θ (K)
1 (Ce)	3.54	2.74	3.62 ($^2F_{5/2}$)	1.77	–43
2 (Pr)	4.92	3.07	5.11 ($^3H_4$)	3.56	–53
3 (Nd)	5.00	3.51	5.20 ($^4J_{9/2}$)	3.96	–83
5 (Eu)	6.46	1.00	–	–	

Magnetic Measurements

Temperature dependencies of the magnetic moment and inverse magnetic susceptibility ($1/\chi$) for complexes **1**–**3** and **5** are shown in Figure 3 and Table 3. For all investigated complexes except for those with europium, values of μ_{eff} at 300 K are in good agreement with theoretical values for a system of two paramagnetic Ln^{3+} cations in the ground state with the corresponding term.[11] When the temperature

is lowered to 5 K, the magnetic moments of complexes Ce, Pr, and Nd are reduced to 2.74–3.51 Bohr magnetons (B.M.). The temperature dependence of $1/\chi(T)$ in the temperature range 120–300 K for the complexes of Ce, Pr, and Nd is linear and well described by the Curie–Weiss law with the parameters given in Table 3. For the europium complex, the value of μ_{eff} at 300 K is 6.46 B.M. (4.24 B.M. per Eu^{3+} ion), which is higher than the typical value for the Eu^{3+} ion (3.6 B.M.). With decreasing temperature μ_{eff} gradually decreases, reaching a value of 1.00 B.M. at 5 K. This μ_{eff}–(T) dependence is explained by the fact that the ground state of Eu^{3+} is a singlet, and there are close levels with different J states, the population of which varies with temperature; therefore, the Curie–Weiss law does not hold.

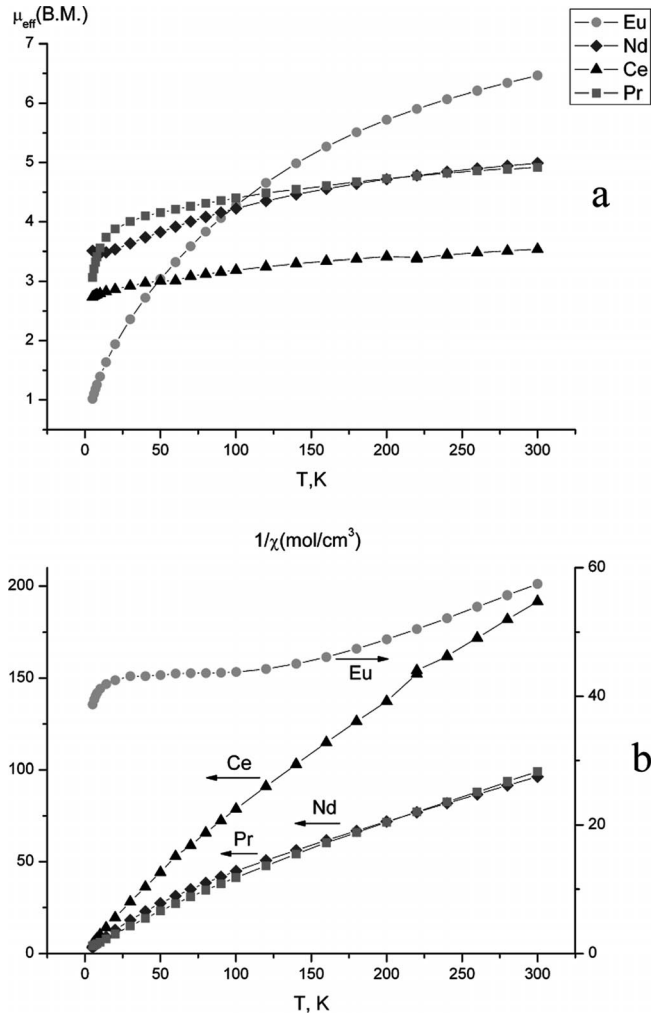

Figure 3. Temperature dependencies of magnetic moment (a) and inverse magnetic susceptibility (b).

Magnetic interactions between paramagnetic centers (two atoms of lanthanide) in the investigated compounds become apparent at temperatures lower than 40–50 K, and at temperatures above 100 K, the magnetic susceptibility of the complexes corresponds well to the presence of two non-interacting paramagnetic centers.

Thermal Properties

Thermal decomposition of complexes begins at temperatures of 40–100 °C. In all cases, the DTA curves show endothermic heat effects in the temperature range 100–160 °C, the weight loss approximately corresponding to the solvated molecules of the organic compounds. These beginning decomposition stages are mostly distinct for the thermal decomposition of heterometallic complex **1** containing cerium (Figure 4).

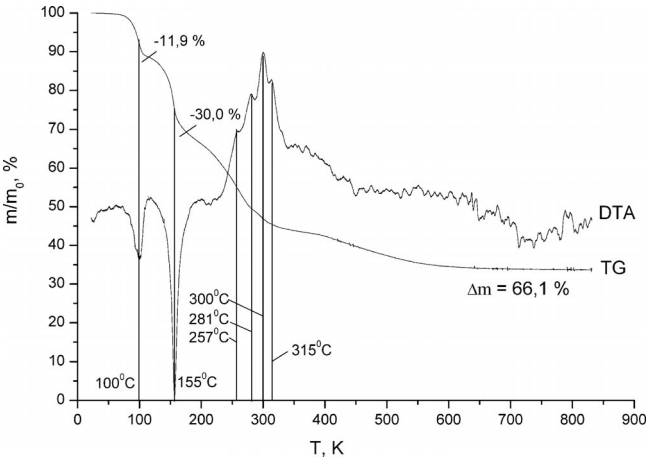

Figure 4. TG and DTA curves for the thermal decomposition of Ce complex.

The first endothermic effect at 100 °C is accompanied by a weight loss (11.9%) corresponding to 2.5 pyridine molecules. The weight loss after the second endothermic effect (155 °C, 30.0%) is in good agreement with removal of all pyridine molecules including the coordinated one. In the temperature range 230–360 °C, decomposition of the complex is accompanied by a strong exothermic effect, and up to four peaks corresponding to intermediate stages can be selected on the DTA curve. According to literature data the decomposition of the Ru–NO fragment in various complexes takes place in a temperature range from 300 to 400 °C.[12] Thus, we suppose that the set of exothermic effects in this temperature range corresponds to the decomposition of part of the core of the complex.

Final products of the thermal decomposition were described by powder diffraction analysis; the corresponding crystal phases and crystallite size are shown in Table 4. The only products of decomposition for the cerium complex that can be identified by XRD are metallic ruthenium and cerium(IV) oxide. Weight loss according to thermal gravimetric (TG) data (66.1%) is very close to the theoretical value for the product with formula $2Ru{\cdot}2CeO_2$ (66.0%). The solid residue after decomposition of the praseodymium complex contains phases of Ru, $PrRuO_3$, $Pr_2Ru_2O_7$, and $(Pr,Ru)_7O_{12}$ with a mass ratio of 25:45:9:21, respectively. $PrRuO_3$ has perovskite-like structure similar to orthorhombic perovskites $MRuO_3$ (M = Ca, Sr), mixed oxide $Pr_2Ru_2O_7$ has a structure similar to pyrochlore, and the structure of displacement compound $(Pr,Ru)_7O_{12}$ is based on the structure of mixed-valence oxide Pr_7O_{12}. According

to the final mass loss (64.1%), the gross composition of the products is described by the formula $Pr_2Ru_2O_{6.7}$. Taking into account the product ratio determined from XRD analysis, the composition of the displacement compound should be $(Pr_{0.4}Ru_{0.6})_7O_{12}$. The only products of decomposition for the neodymium and europium complexes, according to XRD analysis, are metallic ruthenium and Ln_2O_3 oxides in different phase modifications. In case of neodymium compound **3**, the gross composition of the final products according to TG data well correspond to $Ru_2Nd_2O_3$ (theoretical weight loss 65.3%). For europium complex **5** with structure **II**, the final experimental weight loss is somewhat less than the theoretical, corresponding to a gross composition of $Ru_2Ln_2O_3$ (66.2%). This can be explained by the presence of amorphous phases in the decomposition products or by the low stability of the initial crystalline phases and their partial decomposition at room temperature.

Table 4. Products and the conditions of thermal decomposition for investigated complexes.

Complex	T_{start}	T_{end}	Products	Space group	Crystallite size (nm)	$\Delta m/m$
1	25	830	Ru, CeO_2,	*P*6$_3$/*mmc* *Fm*-3*m*	15–20 30–42	66.1 %
2		740	Ru, $PrRuO_3$, $Pr_2Ru_2O_7$, $(Pr,Ru)_7O_{12}$	P6$_3$/*mmc* *Pnma* *Fd*-3*m* *R*-3	24–33 12–16 37–52 10–16	64.1 %
3		740	Ru, Nd_2O_3 Nd_2O_3	*P*6$_3$/*mmc* *P*-3*m*1 *Ia*-3	5–7 10–15 5–7	65.5 %
5		830	Ru, Eu_2O_3 Eu_2O_3	*P*6$_3$/*mmc* *Ia*-3 *C*2/*m*	7–12 15–23 9–16	62.6 %

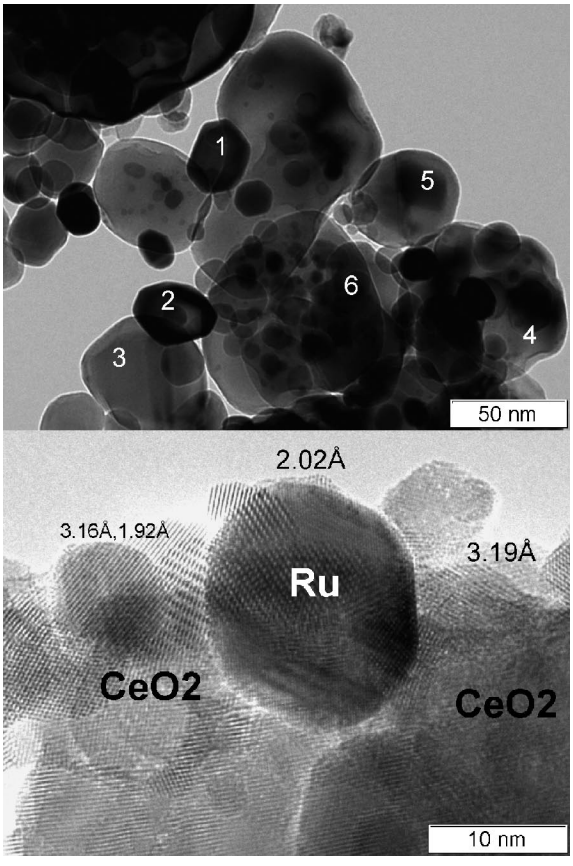

Figure 5. HREM images of the products after the decomposition of the cerium complex. 1, 2: Ru, 3,4: CeO_2, 5,6: Ru + CeO_2.

XRD results for the product of the thermal decomposition of the cerium complex were confirmed by data obtained by high-resolution transmission electron microscopy (HRTEM, Figure 5). The final products of thermolysis are the dense aggregates of metallic ruthenium particles with the size of 3–50 nm and larger particles of CeO_2 (10–200 nm). The product also contains a large individual particles of metallic ruthenium but is basically a ruthenium deposited on cerium oxide. The phases were identified by interplanar distances and EDX-spectra. Size of aggregates range from 100 nm to several microns.

Conclusions

The reaction of $[RuNO(NO_2)_4OH]^{2-}$ with lanthanides can be used to prepare tetranuclear heterometallic complexes with two lanthanide atoms bonded by two ruthenium anions. The decrease in the ionic radius in the sequence Ce, Pr, Nd, Eu results in a transition from the complexes of structure **I** (Ce, Pr, Nd) to complexes of structure **II** (Nd, Eu). Magnetic interactions between two paramagnetic lanthanide centers become significant at temperatures below 50 K, at room temperature, these interactions are negligible. Thermal decomposition of heterometallic lanthanide complexes leads to either mixed oxides (in the case of praseodymium) or a mixture of lanthanide oxide and ruthenium. According to HRTEM analysis, the product of decomposition of the cerium complex mainly consists of metallic ruthenium located on the surface of larger particles of CeO_2.

Experimental Section

Compounds PyH[PyM(NO$_3$){RuNO(NO$_2$)$_4$OH}$_2$M(NO$_3$)$_2$]·X [(1) M = Ce, X = 4Py; (2) M = Pr, X = 4.5Py; (3) M = Nd, X = 2.5Py·C$_3$H$_6$O] and [PyEu(NO$_3$){RuNO(NO$_2$)$_4$OH}$_2$Eu(H$_2$O)NO$_3$]·5Py·C$_3$H$_6$O (5): A solution of $Na_2[RuNO(NO_2)_4OH]\cdot 2H_2O$ (1×10^{-4} mol, 0.041 g) and $Ln(NO_3)_2\cdot 6H_2O$ (1×10^{-4} mol, 0.044 g) in acetone (3 mL) was stirred at room temperature for 40 min. After separation of the $NaNO_3$ precipitate, pyridine (200 mg, 2.6×10^{-3} mol) was added to the filtrate, and the solution was stirred for 20 min. Then hexane (10 mL) was added to the cold reaction mixture and after 1–2 h little yellow (Pr), green-yellow (Nd, Eu), or dark-red (Ce) crystals were obtained with yields of 70–80%. $C_{30}H_{33}Ce_2N_{19}O_{29}Ru_2$ (1606.08): calcd. C 22.4, H 2.1, N 16.6; found C 22.8, H 2.1, N 17.3. $C_{32.5}H_{34.5}N_{19.5}O_{29}Pr_2Ru_2$ (1646.20): calcd. C 23.7, H 2.1, N 16.6; found C 23.9, H 2.6, N 16.9. $C_{25.5}H_{30.5}N_{17.5}Nd_2O_{29}Ru_2$ (1536.74): calcd. C 19.7, H 1.9, N 15.8; found C 20.7, H 2.2, N 15.3. $C_{33}H_{40}Eu_2N_{18}O_{28}Ru_2$ (1642.84): calcd. C 24.1, H 2.4, N 15.4; found C 24.6, H 2.5, N 15.1. IR spectra: $\tilde{\nu}$ = 3452 ν(OH), 1870 ν(NO), 1448 $\nu_{as}(NO_2)$, 1294 $\nu_s(NO_2)$, 833 $\delta(NO_2)$ cm^{-1} for **1**. $\tilde{\nu}$ = 3466 ν(OH), 1869 ν(NO), 1448 $\nu_{as}(NO_2)$, 1294 $\nu_s(NO_2)$, 832 $\delta(NO_2)$ cm^{-1} for **2**. $\tilde{\nu}$ = 3475

ν(OH), 1867 ν(NO), 1450 $\nu_{as}(NO_2)$, 1293 $\nu_s(NO_2)$, 833 $\delta(NO_2)$ cm^{-1} for **3**. $\tilde{\nu}$ = 3493 ν(OH), 1853 ν(NO), 1452 $\nu_{as}(NO_2)$, 1294 $\nu_s(NO_2)$, 833 $\delta(NO_2)$ cm^{-1} for **5**.

$[PyNd(NO_3)\{RuNO(NO_2)_4OH\}_2Nd(H_2O)NO_3]\cdot 5Py\cdot CH_2Cl_2$. (4): To a mixture of solid $Na_2[RuNO(NO_2)_4OH]\cdot 2H_2O$ (0.0414 g, 1×10^{-4} mol) and $Nd(NO_3)_2\cdot 6H_2O$ (0.0440 g, 1×10^{-4} mol) in dichloromethane (3 mL), was added excess pyridine (0.2 mL) with stirring over 20–30 min by 0.03 mL portions. The solid residue was filtered. Several crystals of **4** were separated from the solution after slow diffusion of diethyl ether into the reaction mixture over 1–2 days at 273 K. The same technique was also applied for the cerium and praseodymium nitrates, but only complexes **1** and **2** were separated with yields of 30–40% and identified by elemental analysis, IR spectroscopy, and single-crystal X-ray diffraction. All of the prepared complexes slowly lose weight at room temperature, because of removal of solvent molecules, so for thermal analysis, elemental analysis, and magnetic measurements, we used only freshly prepared samples.

Thermal Analysis: The complexes were studied with a Netzsch STA 409 PC Luxx thermoanalyzer, Al_2O_3 powder being used as standard. The initial weights of the samples were in the range 20–25 mg. The experiments were run in an open alumina crucible in a stream of helium at a heating rate of 10 K/min. The final temperatures of the experiments are reported in Table 4. Analysis of thermal data was performed with Proteus analysis software.[13]

Magnetic Measurements: Magnetic measurements on polycrystalline samples were carried out with a SQUID (Quantum Design) magnetometer at the 5 K and room temperature in an external magnetic field of up to 40 kOe.

Single-Crystal and Powder X-ray Diffraction Analysis: Single crystals of complexes **1**–**5** suitable for X-ray diffraction analysis were obtained by slow diffusion of hexane or diethyl ether into solutions of the complexes in acetone or CH_2Cl_2. Single-crystal X-ray diffraction studies were carried out with a BRUKER X8 APEX CCD diffractometer at room temperature by using graphite-monochromated Mo-K_α radiation (λ = 0.71073 Å). The absorption was corrected with the SADABS program.[14] All structures were solved by means of direct methods and refined by full-matrix least-squares techniques with the SHELXTL program.[14] Hydrogen atoms were calculated to their idealized positions and were refined as riding atoms. Selected distances are shown in Tables 1 and 2. Polycrystalline samples were studied in the 2θ range 5–120° with a DRON RM4 powder diffractometer equipped with a Cu-K_α source (λ = 1.5418 Å) and graphite monochromator at the diffracted beam. Indexing of the diffraction patterns was carried out using data for pure metals and compounds reported in the JCPDS-ICDD database.[15] Unit cell parameters were refined by the full-profile technique within the whole diffraction range with the POWDERCELL 2.4 program.[16] Crystallite sizes of the prepared bimetallic powders were determined by Fourier analysis of single diffraction peaks (the program WINFIT 1.2.1[17]).

Electron Microscopy: HRTEM (high resolution transmission electron microscopy) micrographs were obtained with a JEM-2010 (JEOL, Japan) instrument with a lattice resolution of 0.14 nm and accelerating voltage of 200 kV. The samples for the TEM study were prepared by ultrasonic dispersing in ethanol and consequent deposition of the suspension upon a "holey" carbon film supported on a copper grid. Local elemental analysis was performed with the EDX method with an Energy-dispersive X-ray Phoenix Spectrometer equipped with a Si (Li) detector with an energy resolution not worse than 130 eV.

CCDC-853444, -853445, -853446, -853447, and -853448 contain the supplementary crystallographic data for this paper. These data can be obtained free of charge from The Cambridge Crystallographic Data Centre via www.ccdc.cam.ac.uk/data_request/cif.

Supporting Information (see footnote on the first page of this article): Information on crystal data and refinement parameters.

Acknowledgments

The investigation was partially supported by the Russian Foundation of Basic Research (11-03-00668-a).

[1] a) P. Coppens, I. Novozhilova, A. Kovalevsky, *Chem. Rev.* **2002**, 861–883; b) S. Ferlay, H. W. Schmalle, G. Francese, H. Stoeckli-Evans, M. Imlau, D. Schaniel, T. Woike, *Inorg. Chem.* **2004**, *43*, 3500–3506; c) D. Schaniel, T. Woike, B. Delley, C. Boskovic, K. Krämer, D. Biner, H. U. Güdel, *Phys. Chem. Chem. Phys.* **2005**, *7*, 1164–1170; d) G. F. Caramori, G. Frenking, *Organometallics* **2007**, *26*, 5815–5825; e) A. Zangl, P. Klufers, D. Schaniel, T. Woike, *Inorg. Chem. Commun.* **2009**, *12*, 1064–1066.

[2] a) D. Schaniel, M. Imlau, T. Weisemoeller, *Adv. Mater.* **2007**, *19*, 723–726; b) B. Cormary, I. Malfant, L. Valade, *J. Sol-Gel Sci. Technol.* **2009**, 19–23.

[3] a) L. A. Kushch, L. S. Plotnikova, Yu. N. Shvachko, V. A. Emel'yanov, E. B. Yagubskii, G. V. Shilov, S. M. Aldoshin, *J. Phys. IV Fr.* **2004**, 459–462; b) D. Schaniel, T. Woike, L. L. Kushch, E. Yagubskii, *Chem. Phys.* **2007**, *340*, 211–216; c) L. A. Kushch, S. Golhen, O. Cador, E. B. Yagubskii, M. A. Il′in, D. Schaniel, Th. Woike, L. Ouahab, *J. Cluster Sci.* **2006**, *17*, 303–315; d) L. A. Kushch, L. S. Kurochkina, E. B. Yagubskii, G. V. Shilov, S. M. Aldoshin, V. A. Emel'yanov, Yu. N. Shvachko, V. S. Mironov, D. Schaniel, T. Woike, C. Carbonera, C. Mathonière, *Eur. J. Inorg. Chem.* **2006**, 4074–4085; e) R. B. Morgunov, A. I. Dmitriev, F. B. Mushenok, É. B. Yagubskí, L. A. Kushch, A. R. Mustafina, V. A. Burilov, A. T. Gubádullin, A. I. Konovalov, I. S. Antipin, Y. Tanimoto, *Phys. Solid State* **2009**, 2095–2100.

[4] a) O. Thinon, F. Diehl, P. Avenier, Y. Schuurman, *Catal. Today* **2008**, *137*, 29–35; b) M. Safariamin, L. H. Tidahy, E. Abi-Aad, S. Siffert, A. Aboukais, *C. R. Chim.* **2009**, *12*, 748–753; c) P. Zonetti, R. Landers, A. Cobo, *Appl. Surf. Sci.* **2008**, 6849–6853; d) S. Aouad, E. Abi-Aad, A. Aboukais, *Appl. Catal. B* **2009**, 249–256.

[5] S. Petrovic, V. Rakic, D. M. Jovanovic, A. T. Baricevic, *Appl. Catal. B* **2006**, 249–257.

[6] M. Ito, Y. Yasui, M. Kanada, H. Harashina, S. Yoshii, K. Murata, M. Sato, H. Okumura, K. Kakurai, *J. Phys. Chem. Solids* **2001**, *62*, 337–341.

[7] a) C. Sakai, Y. Doi, Y. Hinatsu, *J. Alloys Compd.* **2006**, *408–412*, 608–612; b) Y. Shimoda, Y. Doi, M. Wakeshima, Y. Hinatsu, *J. Solid State Chem.* **2010**, *183*, 33–40.

[8] D. Y. Chen, M. K. Wu, N. G. Parkinson, C.-H. Du, P. D. Hatton, F. Z. Chien, C. Ritter, *Phys. C: Superconductivity* **2000**, 2157–2158.

[9] a) O. A. Plyusnina, V. A. Emel'yanov, I. A. Baidina, P. E. Plyusnin, S. A. Gromilov, *J. Struct. Chem.* **2011**, *52*, 140–150; b) M. A. Il'in, N. V. Kuratieva, O. A. Kirichenko, I. A. Baidina, D. Yu. Naumov, I. V. Korolkow, V. A. Emel'yanov, *Acta Crystallogr., Sect. E* **2005**, *61*, 126–128, E 61, Part 06.

[10] a) G. A. Kostin, A. O. Borodin, N. V. Kuratieva, *J. Struct. Chem.* **2010**, *51*, 582–584; b) G. A. Kostin, A. O. Borodin, Yu. V. Shubin, N. V. Kurat'eva, V. A. Emelyanov, P. E. Plyusnin, M. R. Gallyamov, *Russ. J. Coord. Chem.* **2009**, *35*, 57–64; c) G. Kostin, A. Borodin, V. Emel'yanov, D. Naumov, A. Virovets, M.-M. Rohmer, A. Varnek, *J. Mol. Struct.* **2007**, *837*, 63–71.

[11] N. Greenwood, A. Earnshaw, *Chemistry of the Elements 2nd ed.*, Butterworth-Heinemann, Oxford, **1997**.
[12] a) M. Matikova-Mal'arova, R. Novotna, Z. Travnicek, *J. Mol. Struct.* **2010**, *977*, 203–209; b) O. A. Plyusnina, V. A. Emel'yanov, I. A. Baidina, I. V. Korol'kov, S. A. Gromilov, *J. Struct. Chem.* **2007**, *48*, 114–121.
[13] *Netzsch Proteus Thermal Analysis v.4.8.1.*, Netzsch-Gerätebau, Bayern, Germany, **2005**.
[14] G. M. Sheldrick, *SHELXL 97*, *Program for Crystal Structure Refinement*, University of Göttingen, Germany, **1997**.
[15] *PCPDFWin, V. 1.30, JCPDS ICDD*, Swarthmore, PA, USA, **1997**.
[16] W. Kraus, G. Nolze, POWDERCELL 2.4, *Program for the Representation and Manipulation of Crystal Structures and Calculation of the Resulting X-ray Powder Patterns*, Federal Institute for Materials Research and Testing, Berlin, Germany, **2000**.
[17] An interactive Windows program for profile fitting and size/strain analysis: S. Krumm, *Mater. Sci. Forum* **1996**, *183*, 228.

Received: November 22, 2011
Published Online: March 16, 2012

